Journal of Magnetic Resonance **144,** 200–206 (2000)
doi:10.1006/jmre.2000.2038, available online at http://www.idealibrary.com on IDEAL®

One-Dimensional Imaging with a Palm-Size Probe

Pablo J. Prado,* Bernhard Blümich,†,[1] and Udo Schmitz†

*Quantum Magnetics, Inc., 7740 Kenamar Court, San Diego, California 92121; and †Institut für Technische und Makromolekulare Chemie, RWTH Aachen, Worringerweg 1, Aachen, D-52056, Germany

Received July 9, 1999; revised January 26, 2000

A new portable magnetic resonance imaging device was built. Spatially resolved NMR was achieved by placing a gradient coil pair and a Helmholtz pair type radio-frequency probe in the gap between two antiparallel polarized permanent magnets. The flat face of the low-field (ν_{proton} = 20 MHz) apparatus allowed for the study of arbitrarily large objects *in situ.* **Relaxation time weighted 1D images were achieved over a 15-mm field of view by a single-point spin-echo sequence. A phase encoding time on the order of 200 μs permited the scanning of a wide range of heterogeneous materials.** © 2000 Academic Press

Key Words: **MRI; NMR; mobile probe; elastomers.**

INTRODUCTION

The concept of inside-out NMR (*1–3*) has been widely used for low spectral resolution applications. NMR tools have been devoted to near-surface studies of arbitrarily large objects. Successful applications include geophysical exploration (*1, 4*) such as groundwater and oil-well logging (*5*), contents of organic solids (*3*), assessment of water in concrete bridge decks (*6*), polymeric materials (*6, 7*), and medical diagnosis (*8*).

Recent reports have shown the benefits of a simple design palm-size NMR probe, the so-called NMR-MOUSE (mobile universal surface explorer) (*7, 9–12*) based on a concept similar to the scanner presented by Matzkanin (*2*). This relatively low frequency device (typically $B_0 < 0.5$ T) allows for the measurement of NMR parameters *in situ* with an approximately one kilogram scanner attached to a small size PC-console setup. Aside from on-line quality control applications, valuable chemical and physical information is retrieved for a wide range of materials. Just as in a conventional in-magnet experiment, relaxation times (*10, 11, 13*), signal intensity, and diffusion constants can be correlated to molecular dynamics and mobility, and to chemical and mechanical properties of a sample in a noninvasive fashion. Fields of study include a wide range of heterogeneous specimens with diverse compositions such as polymers, soft tissues, food products, and porous media.

Achieving spatial resolution with a palm-size NMR probe has the advantage of providing a nondestructive mobile scanning tool that renders information *in situ,* which is otherwise not attainable by other methods. Spatial localization has previously been achieved employing the MOUSE by different procedures. A lateral-direction profile can be acquired by displacement of the probe over the sampled surface (*7, 10*). Millimeter scale resolution is associated to this process due to the finite dimensions of the monitored sensitive volume. In addition, relative signal intensity after repositioning of the scanner may be unreliable owing to the highly inhomogeneous static and excitation fields and the load dependency of the probe tuning. Depth selectivity (y direction) can benefit from the rapidly decaying strength of the static magnetic field (ca. 10 T/m). Although the sensitive region is not flat, relaxation times can be determined for different depths into a sample (*13*) by retuning the radio frequency (rf) probe at the expense of relative signal amplitude manipulation. The outward vanishing of the rf field has been used for rotating frame imaging. This method suffers from low sensitivity, but it has been successfully applied using a large number of averaged scans.

The addition of a single-axis magnetic field gradient coil to the MOUSE improves the lateral spatial resolution (to the order of 100 μm) and introduces the possibility of obtaining a centimeter scale field of view without repositioning of the probe. The benefits of this novel procedure include relaxation time weighted profiles, diffusion constant, and spin interaction assessment and the follow-up of dynamical processes. A quantification of the effect of the excitation pulses in the presence of controlled gradients requires the determination of the sensitive volume (*14*), which can be attained empirically by scanning homogeneous specimens. When imaging using a gradient coil pair in the MOUSE, spin-echo methods are affected by the highly inhomogeneous static and excitation fields. This feature does not allow for pure Hahn or solid echo conditions along the entire field of view. Thus, the acquired profile is a function of the sensitive volume characteristics and the system response to different excitation pulses. Once the fields are determined, this effect can be used to one's advantage in assessing the spin-system interactions.

The present work is aimed to describe the advantages of achieving MRI with a portable low-cost probe and to show the advantages of applying a controlled magnetic field gradient to characterize a heterogeneous specimen through NMR parameters. The scope of the technique is presented through imaging

[1] To whom correspondence should be addressed.

1090-7807/00 $35.00

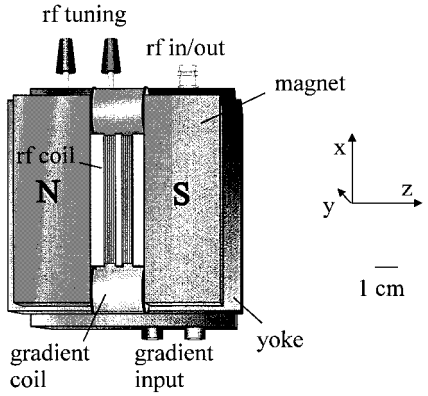

FIG. 1. Top view of the MRI probe based on the NMR-MOUSE. The Helmholtz pair rf coil excites an elongated region along the center of the gap. A pair of antiparallel solenoid coils generates a uniform gradient along the gap and over a ca. 16-mm field of view. The portable MRI probe weighs 1.2 kg. The imaging process was controlled by a Bruker DSX console.

of a series of rubber samples. A detailed calculation of the sensitive volume for a particular probe configuration will be reported elsewhere (*14*).

EXPERIMENTAL

Static and Radio-Frequency Fields

The characteristics of the NMR-MOUSE have been reported previously (*7, 10*). For the prototype presented in this work (Fig. 1), the static polarizing magnetic field $\mathbf{B}_0$ is produced by antiparallel NdFeB permanent magnets (Dexter Magnetic Materials, GmbH, Planegg, Germany). The resulting field lines at the scanner surface are oriented approximately across the magnets gap (z direction), and its strength decreases rapidly in the outward direction. The rf excitation field $\mathbf{B}_1$ is produced by a coil positioned in the MOUSE gap which generates predominantly y components, i.e., those perpendicular to the static field.

A new MOUSE-based probe was built to achieve 1D spatial resolution and then perform MRI studies (Fig. 1). The portable imager is characterized by fine resolution (~100 μm) and an extended field of view (16 mm long, approximately 2 mm wide, and under 0.5 mm thick). The MRI-MOUSE was constructed using rectangular block permanent magnets separated by a 14-mm gap (proton Larmor frequency at surface = 20.1 MHz). With this configuration, the smallest static field gradient is along the gap (x direction). This is thus the selected dimension for imaging because it allows for the largest field of view. Although the point of null derivatives,

$$\frac{\partial B_z}{\partial x} = \frac{\partial B_z}{\partial y} = \frac{\partial B_z}{\partial z} = 0, \qquad [1]$$

is located between the magnets, a nonuniform sensitive volume can be generated near the probe.

A LakeShore Hall sonde (0.2 mm width, 0.01 mT precision) was used for scanning the polarizing magnetic field. The sonde was driven by a LakeShore 420 Gaussmeter and displaced in a plane 0.5 mm above the probe surface by a Roland DG DXY-880A plotter. The monitoring and acquisition processes were controlled by PC-based software (B-field Scanner). Figure 2a shows a contour map of the z component of $\mathbf{B}_0$. Closed contours are produced by reorientation of the field lines as the edge of the magnet is approached. The B_{0z} component along the center of the gap is plotted in Fig. 2b. This behavior dictates the maximum field of view attained by the imaging procedure. The overall change on B_{0z} along the sensitive volume is under 1 T/m, which compares to ca. 10 T/m in the y direction. The stray-field selective depth (*15, 16*) is associated with pulse durations under 10 μs. This highly inhomogeneous polarizing field does not allow one to retrieve chemical shift information.

The rf field is produced by a Helmholtz pair coil (monolayer, multiturn) (Fig. 1), which generates an elongated excited region following the gap between the individual sections. The acoustic ringing is under 40 μs. We noticed that coils with

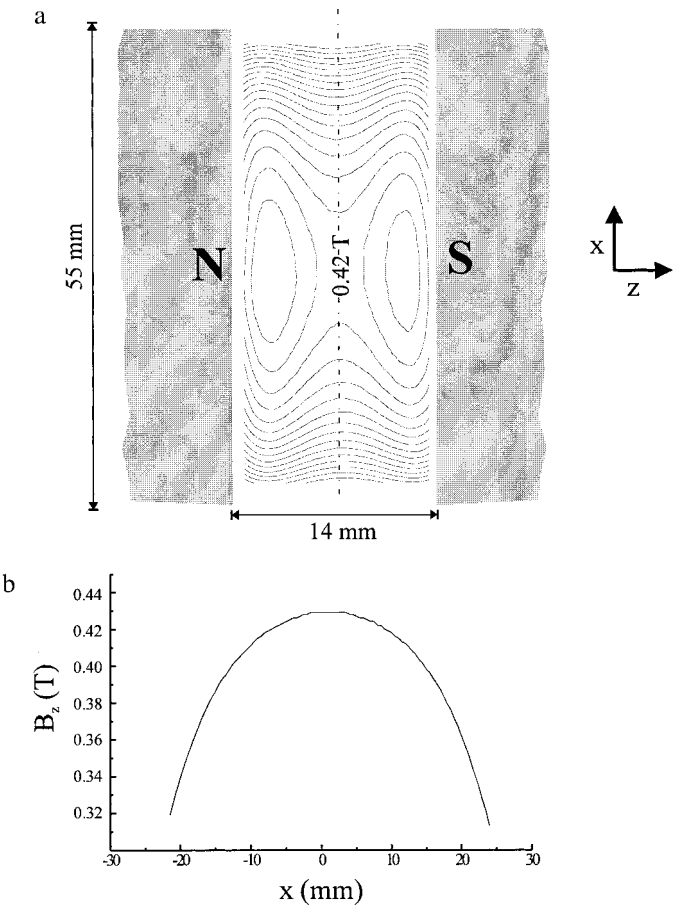

FIG. 2. Map of the z component (across the magnets gap) amplitude of the polarizing magnetic field at 0.5 mm from the probe's surface: (a) contour plot with a magnetic field strength increment of 8 mT per level, (b) profile along the center of the gap.

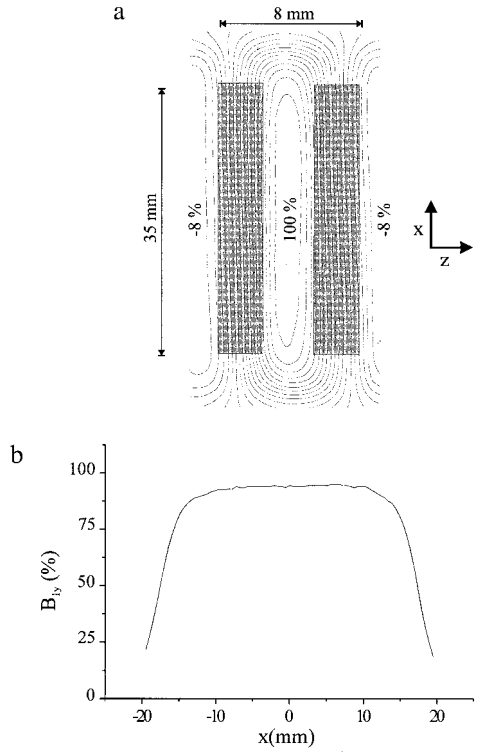

FIG. 3. Bench test (dc) of the *y* component (outward from probe) of the magnetic field produced by the Helmholtz pair coil used for rf excitation: (a) contour plot of measured data, (b) profile along the center of the gap.

additional layers of wires were prone to arcing due to the high voltage difference among the layers resulting from the long turn design. The *y* component of the rf field was measured near the surface of the probe by the Hall probe scanner mentioned above. The rf coil has an inductance of $L = 3.5\ \mu$H and a loaded quality factor of $Q = 70$. Short excitation pulses can be generated (2 μs at under 200 W), and the tuning is significantly sensitive to probe loading (*17*). Figure 3 shows the B_{1y} component strength measured in 0.2 mm steps. This excitation field is homogeneous over a 30-mm region along the gap and decays across the gap to 50% of its maximum strength at 2 mm from the center line. Surface-grounded probes with a low sensitivity to loading are currently being tested.

Initial tests to measure the sensitive volume were performed by displacing a 1-mm wide natural rubber sample over the probe. A sensitivity range of around 16 mm is estimated by the signal magnitude dependence with scanning sample positioning. Because of the response of the spin system to the strength and direction of the magnetic fields, the profile can be modulated by the choice of the examining sample. This phenomenon is discussed with more detail below.

Gradient Coil

Spatial resolution along the magnets gap was achieved by two 10-mm diameter 100-turn multilayer solenoid antiparallel gradient coils (Figs. 1 and 4a). Due to the presence of heterogeneous static magnetic fields, a phase encoding imaging sequence was employed by varying the field gradient strength along the *x* direction.

Given that this probe is mobile and usually repositioned by an operator's direct handling, the gradient-coil's copper-wire winding specifications were determined by maintaining a low power threshold. This bears a twofold advantage, i.e., safety and minimal size of the driving power amplifiers. The current-generated magnetic field produced by the coil pair was measured with the Hall probe as described in the preceding section. This monitoring was performed by placing the coils in a holder prior to the positioning at the edge of the magnets gap. Figure 4a shows a contour plot of the *z* component of the added magnetic field. A maximum strength of 0.85 mT/A was measured above each coil. The current at continuous rate had to be kept under 0.7 A due to heat dissipation limitations. The derivative $\partial B_z/\partial x$, was calculated and the fitted line is displayed in Fig. 4b. The region for the least squares fitting is

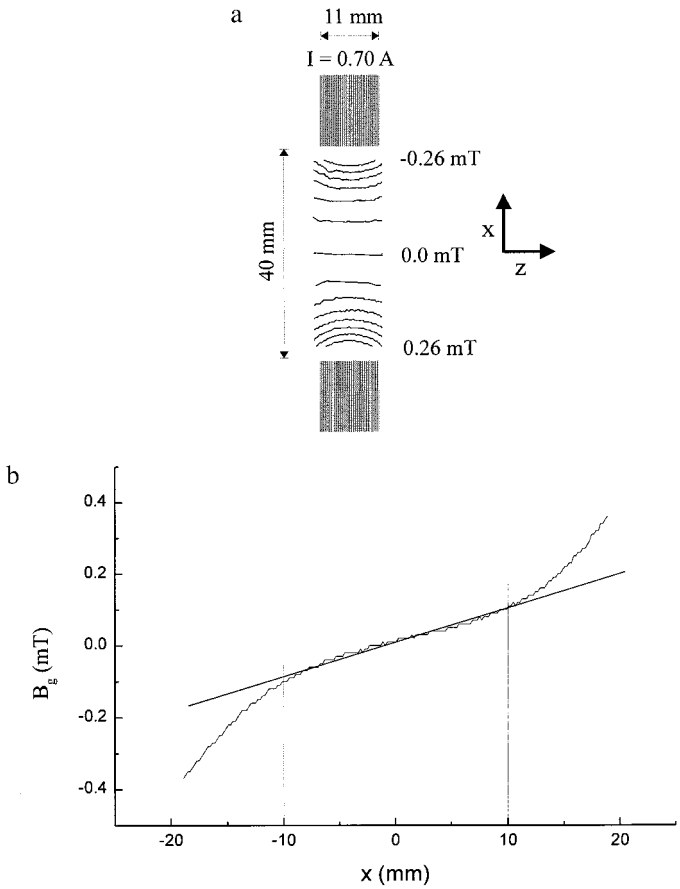

FIG. 4. Performance of the gradient coil in a bench test ($I = 0.7$ A): (a) contour map of the *z* component of the added field with a 0.04 mT change between levels, (b) current driven magnetic field gradient along the center of the magnet's gap. The straight line on the graph represents a least-squares linear fit to the data in the indicated region. A constant gradient of $G_x = \partial B_{gz}/\partial x = 0.0138(3)$ T/(m A) was computed.

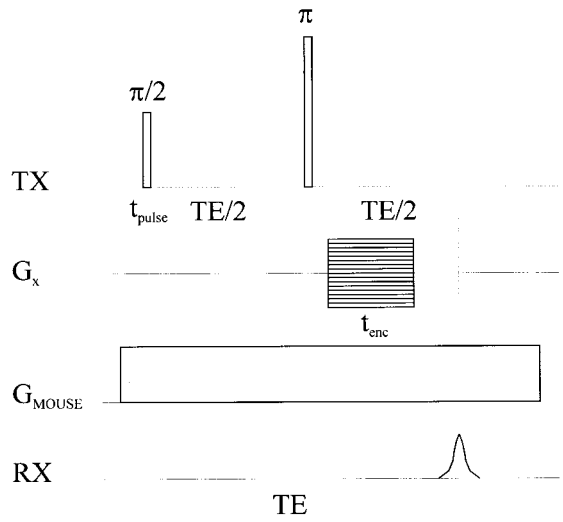

FIG. 5. Single-point spin-echo imaging sequence used for scanning of the *k* space by pure phase encoding. The data are collected at the echo time in the presence of inhomogeneous underlying magnetic fields.

indicated (−10 to 10 mm) and a gradient of $G_x = 0.0138(3)$ T/(m A) was computed.

The MRI performance of the new coils is presented below. Evaluations of linearity, switching delay time, and maximum strength are discussed based on spin-echo imaging tests.

Imaging Method: Single-Point Phase Encoding

When a hard rf pulse is applied, the excited volume can be assessed by the pulse frequency span ($\Delta\nu_{pulse} \cong (1/t_{pulse})$). For protons and a 2-$\mu$s rf pulse, the sensitive volume is a low depth ($\Delta y < 1$ mm) elongated ($\Delta x > 15$ mm) region, as can be calculated from the results plotted in Fig. 2a. Neither projection-reconstruction frequency encoding (*18*) nor single-point imaging (*19, 20*) can be performed under the MOUSE static field conditions because signal amplitude vanishes within the probe's dead time. Due to the strength of the present static read gradients and the associated rapid dephasing of the signal, a pure spin echo phase encoding method can be used. The echo–amplitude change with a controlled external gradient (Fig. 5) is detected to scan the reciprocal-space signal.

For a nuclear density distribution $\rho(\mathbf{r})$, if diffusion effects are not significant, the signal after a time t is determined by

$$S(k_x) = \int \rho(\mathbf{r})\exp[i\omega_0(\mathbf{r})t]\exp(ik_x x) \times \exp\left[-\frac{t}{T_2^*(\mathbf{r})}\right]\Delta(\omega_{\rm rf}, \mathbf{r}, t_{\rm pulse})d\mathbf{r}, \quad [2]$$

where G_x is the controlled gradient in the x direction, $\omega_0(\mathbf{r})$ is the frequency distribution resulting from the static polarizing fields, and k_x is the x component of the reciprocal space vector, $\mathbf{k} = \gamma\,\mathbf{G}\,t_{\rm enc}$, and $t_{\rm enc}$ is the encoding time. Δ represents the sensitive volume excited by the hard rf pulse in the presence of a nonuniform field, thus, it is a function of the excitation frequency $\omega_{\rm rf}$, the position, and the pulse length $t_{\rm pulse}$. This factor is responsible for the profile shape even when imaging homogeneous samples. It was demonstrated in the previous section that the added field gradient can be considered constant over the sensitive region.

To ensure excitation of the same volume by both rf pulses generating a Hahn echo (nominal $\pi/2$ and π flip angles), they are set with the same duration but different amplitude. The signal is then detected at the echo time, *TE*, overcoming the effect of strong read gradients. After heterodyne mixing, a weighted profile is obtained by Fourier transformation of this reciprocal space signal,

$$\rho'(x) = |FT[S(k_x)]| \approx \int_y\int_z \rho(x, y, z)\exp\left[-\frac{TE}{T_2(x, y, z)}\right] \times \Delta(\omega_{\rm rf}, x, y, z, t_{\rm pulse})dydz, \quad [3]$$

where the integral is performed over a plane perpendicular to the gradient direction. Computation of the ρ' profile can be attained only when the sensitive volume is determined and will contain information on the spin interactions due to inhomogeneous rf excitation. Calculation of the magnetization-distribution expectation values through a density matrix formalism (*14, 18*) include the rotation operators, which are not constant over the y–z planes. Furthermore, the high inhomogeneity of the polarizing field produces rapid phase and amplitude modulation over the narrow sensitive plane at the x position. One can thus consider the signal-weighted average over the narrow y–z region and evaluate the effect along the field-of-view by a simple experiment with an homogeneous phantom. Then, the observed profile during the single-point spin-echo measurement becomes

$$\rho'(x) \approx \rho(x)\exp\left[-\frac{TE}{T_2(x)}\right]\Delta(\omega_{\rm rf}, x, t_{\rm pulse}). \quad [4]$$

A T_1 contrast weight is realized by pulses preceding the imaging sequence. An additional modulation can be produced during the transient state toward saturation if the time between sampling of k-space points does not allow for full magnetization recovery. This produces two effects, restrictions in signal resolution and spin–lattice image contrast (*21*).

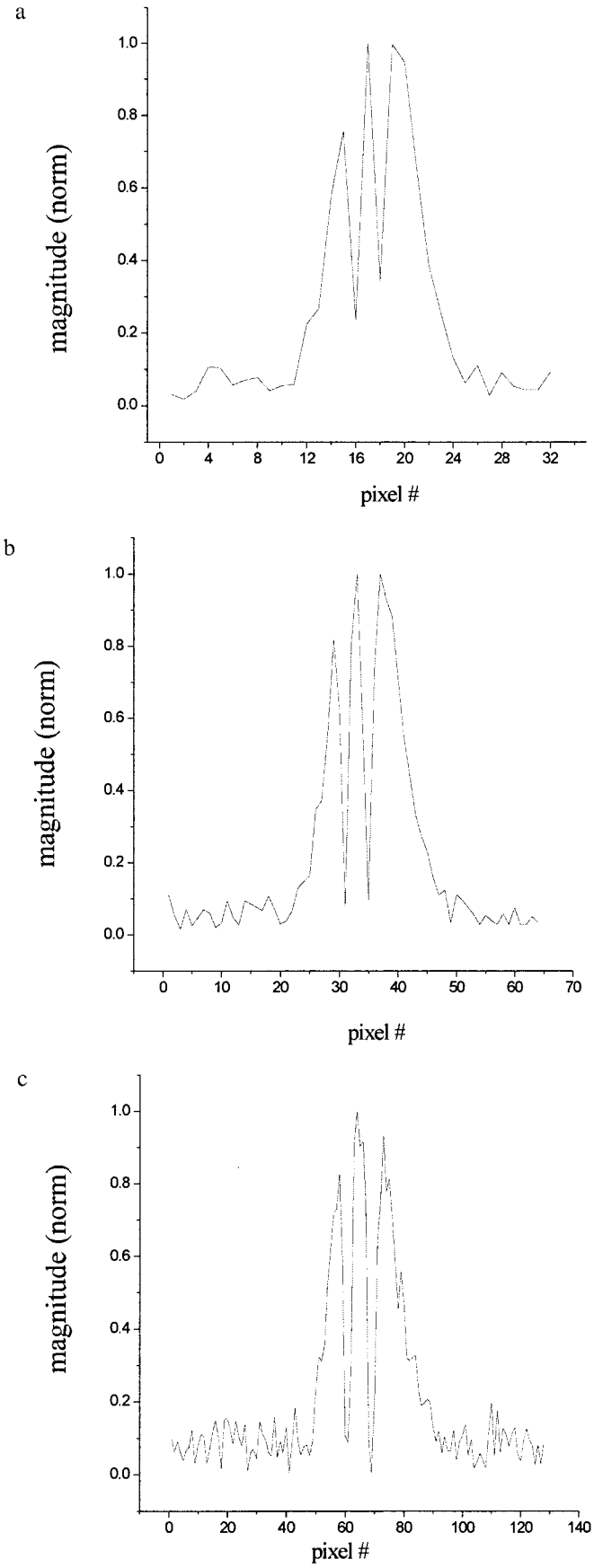

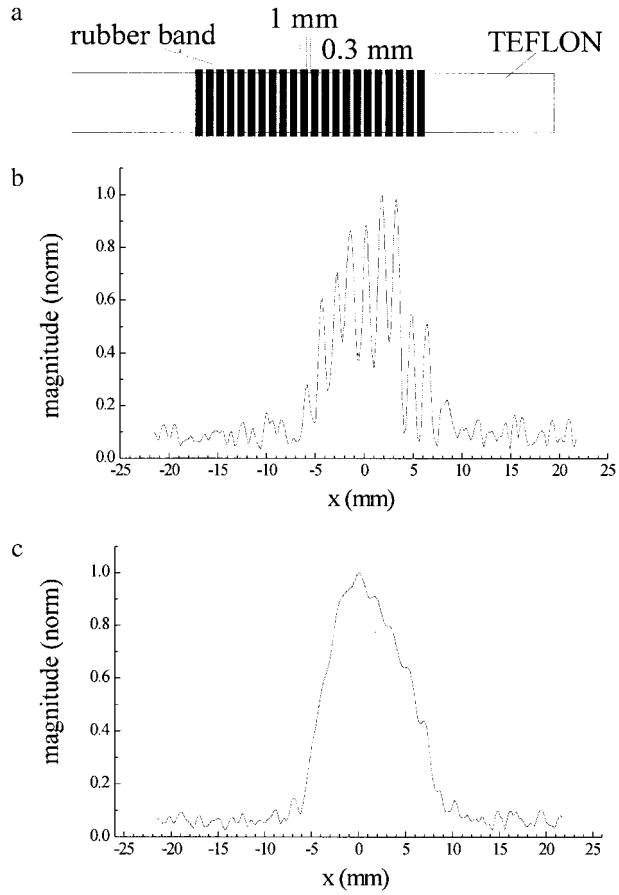

FIG. 7. (a) Multiturn commercial rubber band phantom used in (b), (b) 1D map, and (c) uniform natural rubber specimen larger than the rf coil.

RESULTS AND DISCUSION

Imaging with a portable single-sided probe offers a powerful technique for material science applications. In this respect phase encoding is of great advantage in the imaging process for specimens presenting a fast decaying signal, which are frequently found in solid-like materials and fluids in confined environments. The technique can then be extended to soft tissues and liquids, considering diffusion restrictions (*13*). In order to present the capabilities of the method, a nonvulcanized elastomer and a commercial rubber band were imaged using the MRI-MOUSE. The vulcanized materials had spin–spin relaxation times under 1.5 ms, and thus they required fast gradient switching during phase encoding.

The probe was tuned at 20.1 MHz, corresponding to the near surface frequency ($y < 1$ mm). Rf pulses were calibrated to

FIG. 6. Profiles of a nonvulcanized elastomer with two 1-mm groves separated by a 3-mm gap. The field of view is kept constant by changing the number of gradient steps and maximum amplitude. $t_{enc} = 300$ μs: (a) 32 points, (b) 64 points, and (c) 128 points.

2.2 μs by setting the refocusing pulse amplitude in Fig. 5 at double the amplitude of the initial excitation pulse (*11*). A repetition time of 80 ms allowed for rapid averaging and the fast echo decay required a short encoding delay of under 400 μs. The phase encoding gradients were switched after the second pulse in order to avoid spurious refocusing due to long gradient raise times. The gradient-amplifier power requirement for 64-point profiles over a field-of-view of ca. 20 mm was under 80 W.

Figure 6 shows the scanned profiles for the nonvulcanized elastomer which was prepared with two carved 1-mm groves separated by 3 mm. In all three profiles the phase encoding time was 300 μs and the nonzero filled data were acquired with a 1-μs dwell time and a 500-kHz filter. The spin echoes for Fig. 6a were acquired in 5.8 min for the 32 gradient amplitudes, while for Fig. 6b, 64 spectra were acquired in 58 min, and for the profile in Fig. 6c, 128 spectra were acquired in 250 min. The estimated resolution is 1200, 600, and 300 μm, respectively. Higher sensitivity and improved resolution can be obtained with an appropriated setup. Elongated solenoid coils and repositioning the gradient coils closer to the excitation volume were tested for this purpose. The observed increase in S/N ratio is achieved at expenses of a reduced field-of-view.

A rubber band wrapped on teflon (Figs. 7a and 7b) was used for the *x*-scale calibration. The reciprocal space data were zero-filled to 256 points prior to Fourier transformation. A signal-to-noise ratio of 60 for a homogeneous natural rubber sample (Fig. 7c) was estimated after a 40 min acquisition for the 64 gradient values with an encoding time of 150 μs. Notice that the nonuniform shape of the profile is due to the nonuniform sensitive volume, as explained in the preceding section.

T_2 weighted profiles (Eq. [4]) are obtained by changing the echo time and keeping the encoding time constant. Three natural rubber samples were prepared for this experiment. The rubbers were cut 2 mm thick and positioned with a 2-mm gap among them. Eight different *TE* values were set in the range 0.8 to 4.3 ms. Three of the computed profiles are plotted in Fig. 8a. One hundred twenty-eight points were attained in 14 min per profile. A five-point average for the signal magnitude was calculated for each of the three samples. The signal decay corresponding to that of the samples is shown in Fig. 8b. A spin–spin relaxation time of $T_2 = 1.1 \pm 0.2$ ms was fitted with a least-square algorithm. The values corresponding to the three specimens are not significantly different, due to the fact that the variations are in the curing time and not in the chemical cross-linking during vulcanization (*12*).

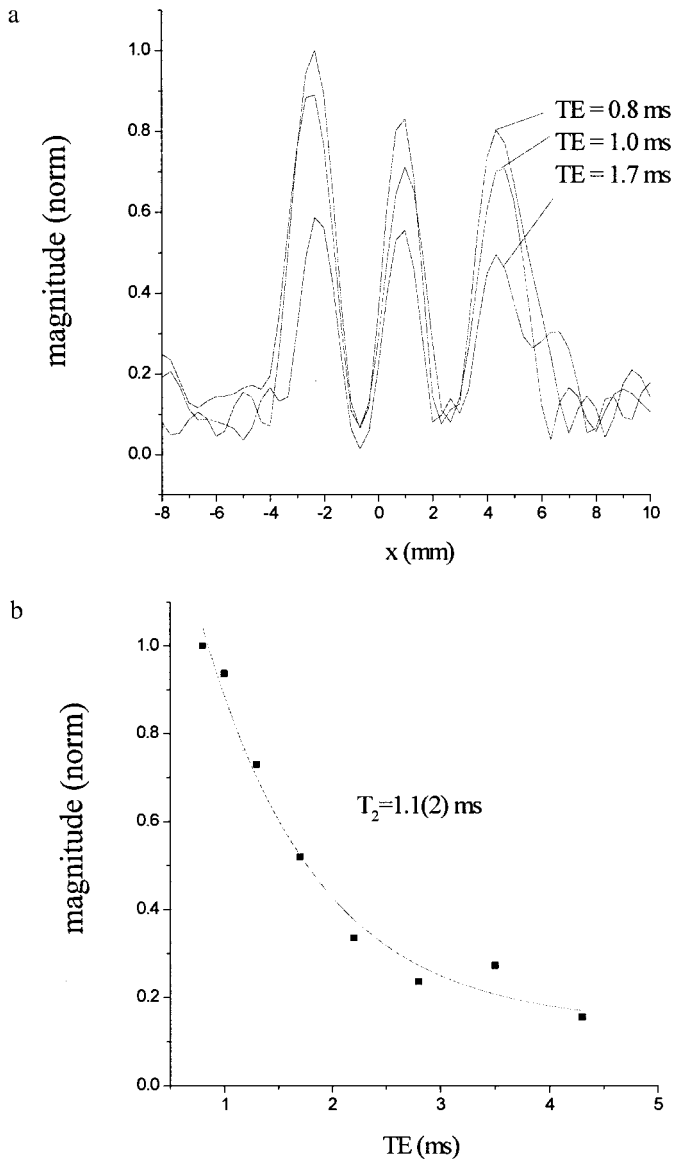

FIG. 8. Set of three 2-mm natural rubber specimens separated by 2-mm gaps: (a) T_2-weighted profiles corresponding to three echo times, (b) signal decay for the left specimen. The full line corresponds to the single-exponential fit to the data.

CONCLUSIONS

A new portable probe for spatially resolved NMR studies was built. A pair of gradient solenoid coils and a Helmholtz pair rf probe positioned in the gap between antiparallel polarizing permanent magnets resulted in profiles over a 15-mm field of view. The weight of the imager probe is about 1 kg and although it was driven by a Bruker DSX console, it can be operated by a small-size NMR system.

The gradient coil produced a close to uniform gradient over the field of view. Due to the highly inhomogeneous underlying static fields, a single-point spin-echo phase encoding sequence was used for the imaging procedure. The potential of the technique was shown by the MRI measurements on heterogeneous rubber specimens, presenting spin–spin relaxation times on the order of 1 ms. T_2 contrast on the profiles was achieved by the data acquisition with different echo delays and constant phase encoding time.

ACKNOWLEDGMENTS

We thank G. Zimmer and F. Balibanu for useful discussions. One of us (P.J.P) thanks the Alexander von Humboldt Foundation for a Research Scientist Fellowship.

REFERENCES

1. R. L. Kleinberg, Well logging, *in* "Encyclopedia of NMR" (D. M. Grant and R. K. Harris, Eds.), pp. 4960–4969, Wiley, New York (1996).
2. G. A. Matzkanin, A review of nondestructive characterization of composites using NMR, *in* "Nondestructive Characterization of Materials" (P. Höller, V. Hauck, C. O. Rutud, and R. E. Green, Eds.), pp. 655–669, Springer, Berlin (1989).
3. W. L. Rollwitz, Using radiofrequency spectroscopy in agricultural applications, *Agricultural Eng.* **66,** 12–14 (1985).
4. A. Sezginer, D. D. Griffin, R. L. Kleinberg, M. Fukuhara, and D. G. Dudley, Very rapid simultaneous measurements of nuclear magnetic resonance spin–lattice relaxation time and spin–spin relaxation time, *J. Magn. Reson. A* **92,** 104–109 (1996).
5. R. L. Kleinberg, A. Sezginer, D. D. Griffin, and M. Fukuhara, A novel NMR apparatus for investigating an external sample, *J. Magn. Reson.* **97,** 466–485 (1992).
6. G. B. Matson, T. Schleich, C. Serdahl, G. Acosta, and J. A. Willis, Measurement of longitudinal relaxation times using surface coils, *J. Magn. Reson.* **56,** 200–206 (1984).
7. G. Eidmann, R. Savelsberg, P. Blümler, and B. Blümich, The NMR-MOUSE, a mobile universal surface explorer, *J. Magn. Reson. A* **122,** 104–109 (1996).
8. E. Fukushima, A. R. T. Rath, and S. B. W. Roeder, U.S. Patent 4721914 (1988).
9. G. Zimmer, A. Guthausen, U. Schmitz, K. Saito, and B. Blümich, Weathering investigation of PVC coating on iron sheets by the NMR MOUSE, *Adv. Mater.* **12,** 987–989 (1997).
10. B. Blümich, P. Blümler, G. Eidmann, A. Guthausen, R. Haken, U. Schmitz, K. Saito, and G. Zimmer, The NMR-MOUSE: Construction, excitation, and applications, *Magn. Reson. Imaging* **16,** 479–484 (1998).
11. A. Guthausen, "Die NMR-MOUSE. Methoden und Anwendungen zur Charakterisierung von Polymeren," Ph. D. thesis, RWTH, Aachen (1998).
12. A. Guthausen, G. Zimmer, P. Blümler, and B. Blümich, Analysis of polymer materials by the NMR-MOUSE, *J. Magn. Reson.* **130,** 1–7 (1998).
13. G. Zimmer, A. Guthausen, and B. Blümich, Characterization of cross-link density in technical elastomers by the NMR-MOUSE, *Solid State NMR* **12,** 183–190 (1998).
14. F. Balibanu, K. Hailu, R. Eymael, D. E. Demco, and B. Blümich, Nuclear magnetic resonance in inhomogeneous magnetic fields, *J. Magn. Reson.,* submitted.
15. P. J. McDonald, Stray field magnetic resonance imaging, *Progr. Nuc. Magn. Reson. Spetrosc.* **30,** 69–99 (1997).
16. A. A. Samoilenko, D. Yu. Artemov, and L. A. Sibeldina, Formation of sensitive layer in experiments on NMR subsurface imaging of solids, *JETP Lett.* **47,** 417–419 (1988).
17. R. A. Assink, E. Fukushima, A. A. V. Gibson, A. R. Rath, and S. Roeder, A nondetuning surface coil, the Semitoroid, *J. Magn. Reson.* **66,** 176–181 (1986).
18. P. T. Callaghan, "Principles of Nuclear Magnetic Resonance Microscopy," Clarendon Press, Oxford (1991).
19. S. Emid and J. H. N. Creyghton, High resolution NMR imaging in solids, *Physica B* **128,** 81–83 (1985).
20. S. Gravina, and D. G. Cory, Sensitivity and resolution of constant-time imaging, *J. Magn. Reson. B* **104,** 53–61 (1994).
21. M. T. Vlaardingerbroek and J. A. den Boer, "Magnetic Resonance Imaging," Springer, Berlin (1996).